Impact of Phase Retrieval on Visualizing the Lumen in Angiographic Phantoms with the use of Polychromatic X-ray Sources

1. Beltran approach

Information of the phase shift (ϕ) and the intensity associated with the absorption (I) are related to the real (δ) and imaginary (β) coefficients of the refractive index by means of the following equations

$$\phi\left(\frac{x}{M},\frac{y}{M},0,E\right)=-k(E)\int_{-z_o}^{0}\delta\left(\frac{x}{M},\frac{y}{M},z',E\right)dz' \tag{S1}$$

$$I\left(\frac{x}{M},\frac{y}{M},0,E\right)=I\left(\frac{x}{M},\frac{y}{M},-z_o,E\right)e^{-2k(E)\int_{-z_o}^{0}\beta\left(\frac{x}{M},\frac{y}{M},z',E\right)dz'} \tag{S2}$$

where M is the geometric magnification of the sample at the detector, E is the energy of X-rays through the sample, k is the wavenumber in vacuum and z_o is the thickness of the sample.

Free Propagation (Inline XPCI)

Characteristic equation: Transport-Intensity equation

$$M^2I(x,y,z_1,E)=I\left(\frac{x}{M},\frac{y}{M},0,E\right)-\frac{z_1}{k(E)}\vec{\nabla}_T\cdot\left[I\left(\frac{x}{M},\frac{y}{M},0,E\right)\vec{\nabla}_T\phi\left(\frac{x}{M},\frac{y}{M},0,E\right)\right] \tag{S3}$$

$$\frac{M^2I(x,y,z_1,E)}{I\left(\frac{x}{M},\frac{y}{M},-z_o,E\right)}=\left[e^{-2k(E)\int_{-z_o}^{0}\beta\left(\frac{x}{M},\frac{y}{M},z',E\right)dz'}+z_1\vec{\nabla}_T\cdot\left[e^{-2k(E)\int_{-z_o}^{0}\beta\left(\frac{x}{M},\frac{y}{M},z',E\right)dz'}\vec{\nabla}_T\int_{-z_o}^{0}\delta\left(\frac{x}{M},\frac{y}{M},z',E\right)dz'\right]\right] \tag{S4}$$

using equations S1 and S2 in equation S3. The total projected thickness of the sample is defined as

$$a_T\left(\frac{x}{M},\frac{y}{M}\right)=a_1\left(\frac{x}{M},\frac{y}{M}\right)+a_2\left(\frac{x}{M},\frac{y}{M}\right) \tag{S5}$$

where the $a_1\left(\frac{x}{M},\frac{y}{M}\right)$ ($a_2\left(\frac{x}{M},\frac{y}{M}\right)$) refers to the projected thickness of the encasing (encapsulated) material. With equation S5 and the following approximation in the integral terms

$$\int_{-z_o}^{0}\delta\left(\frac{x}{M},\frac{y}{M},z',E\right)dz'=\delta_1(E)a_1\left(\frac{x}{M},\frac{y}{M}\right)+\delta_2(E)a_2\left(\frac{x}{M},\frac{y}{M}\right)$$

$$\int_{-z_o}^{0}\delta\left(\frac{x}{M},\frac{y}{M},z',E\right)dz'=\delta_1(E)a_T\left(\frac{x}{M},\frac{y}{M}\right)+\Delta\delta(E)a_2\left(\frac{x}{M},\frac{y}{M}\right) \tag{S6}$$

$$\int_{-z_o}^{0} \beta\left(\frac{x}{M},\frac{y}{M},z',E\right)dz' = \beta_1(E)a_1\left(\frac{x}{M},\frac{y}{M}\right) + \beta_2(E)a_2\left(\frac{x}{M},\frac{y}{M}\right)$$

$$\int_{-z_o}^{0} \beta\left(\frac{x}{M},\frac{y}{M},z',E\right)dz' = \beta_1(E)a_T\left(\frac{x}{M},\frac{y}{M}\right) + \Delta\beta(E)a_2\left(\frac{x}{M},\frac{y}{M}\right) \quad \textbf{(S7)}$$

where $\Delta\delta(E) = \delta_2(E) - \delta_1(E)$ and $\Delta\beta(E) = \beta_2(E) - \beta_1(E)$, equation S4 is written as

$$\frac{M^2 I(x,y,z_1,E)}{I\left(\frac{x}{M},\frac{y}{M},-z_o,E\right)e^{-2k(E)\beta_1(E)a_T\left(\frac{x}{M'}\frac{y}{M}\right)}} = e^{-2k(E)\Delta\beta(E)a_2\left(\frac{x}{M'}\frac{y}{M}\right)} + z_1\Delta\delta(E)\vec{\nabla}_T\cdot\left[e^{-2k(E)\Delta\beta(E)a_2\left(\frac{x}{M'}\frac{y}{M}\right)}\vec{\nabla}_T a_2\left(\frac{x}{M},\frac{y}{M}\right)\right]$$

$$\frac{M^2 I(x,y,z_1,E)}{I\left(\frac{x}{M},\frac{y}{M},-z_o,E\right)e^{-2k(E)\beta_1(E)a_T\left(\frac{x}{M'}\frac{y}{M}\right)}} = \left[1 - \frac{z_1\Delta\delta(E)}{2k(E)\Delta\beta(E)}\nabla_T^2\right]e^{-2k(E)\Delta\beta(E)a_2\left(\frac{x}{M'}\frac{y}{M}\right)} \quad \textbf{(S8)}$$

where $\vec{\nabla}_T e^{-2k(E)\Delta\beta(E)a_2\left(\frac{x}{M'}\frac{y}{M}\right)} = -2k(E)\Delta\beta(E)e^{-2k(E)\Delta\beta(E)a_2\left(\frac{x}{M'}\frac{y}{M}\right)}\vec{\nabla}_T a_2\left(\frac{x}{M},\frac{y}{M}\right)$. Additionally, it is assumed that the total projected thickness varies slowly in the transverse plane, $\vec{\nabla}_T a_T\left(\frac{x}{M},\frac{y}{M}\right) \approx 0 \rightarrow \frac{\partial a_T\left(\frac{x}{M'}\frac{y}{M}\right)}{\partial x\prime} \approx 0$. Although that assumption is violated at the edges of the sample, the retrieving of the projected thickness of the encapsulated material is valid only if it is not located close to the edges. Using discrete Fourier space enables to convert the differential equation S8 into an algebraic equation. The discrete Fourier transforms of each function from equation S8 are

$$F(x,y,E) = \frac{M^2 I(x,y,z_1,E)}{I\left(\frac{x}{M},\frac{y}{M},-z_o,E\right)e^{-2k(E)\beta_1(E)a_T\left(\frac{x}{M'}\frac{y}{M}\right)}} = \frac{1}{N^2}\sum_{u,v=-\frac{N}{2}}^{\frac{N}{2}} f(u,v,E)e^{\frac{2\pi i}{N}(xu+yv)} \quad \textbf{(S9)}$$

$$G(x,y,E) = e^{-2k(E)\Delta\beta(E)a_2\left(\frac{x}{M'}\frac{y}{M}\right)} = \frac{1}{N^2}\sum_{u,v=-\frac{N}{2}}^{\frac{N}{2}} g(u,v,E)e^{\frac{2\pi i}{N}(xu+yv)} \quad \textbf{(S10)}$$

For the Laplacian of the function G, it is considered

$$\nabla_T^2 G(x,y,E) = \frac{\partial^2 G(x,y,E)}{\partial x'^2} + \frac{\partial^2 G(x,y,E)}{\partial y'^2} \quad \textbf{(S11)}$$

A second-order Taylor expansion around the center of mass of an arbitrary pixel (x,y) is used to calculate the function G at the center of mass of its nearest neighboring pixels, at $(x \pm W, y)$ and $(x, y \pm W)$, and to calculate the discrete second derivatives of G as

$$G(x \pm W,y,E) = G(x,y,E) \pm W\frac{\partial G(x,y,E)}{\partial x'} + \frac{W^2}{2}\frac{\partial^2 G(x,y,E)}{\partial x'^2} \quad \textbf{(S12)}$$

$$\frac{\partial^2 G(x,y,E)}{\partial x'^2} = \frac{1}{W^2}[G(x+W,y,E) + G(x-W,y,E) - 2G(x,y,E)] \quad \textbf{(S13)}$$

$$G(x, y \pm W, E) = G(x,y,E) \pm W\frac{\partial G(x,y,E)}{\partial y'} + \frac{W^2}{2}\frac{\partial^2 G(x,y,E)}{\partial y'^2} \quad \textbf{(S14)}$$

$$\frac{\partial^2 G(x,y,E)}{\partial y'^2} = \frac{1}{W^2}[G(x,y+W,E) + G(x,y-W,E) - 2G(x,y,E)] \quad \textbf{(S15)}$$

$$\nabla_T^2 G(x,y,E) = \frac{1}{W^2}[G(x+W,y,E) + G(x-W,y,E) + G(x,y+W,E) + G(x,y-W,E) - 4G(x,y,E)] \quad \textbf{(S16)}$$

$$\nabla_T^2 G(x,y,E) = \frac{1}{W^2N^2}\left[\sum_{u,v=-\frac{N}{2}}^{\frac{N}{2}}\left[e^{\frac{2\pi i}{N}Wu} + e^{-\frac{2\pi i}{N}Wu}\right]g(u,v,E)e^{\frac{2\pi i}{N}(xu+yv)}\sum_{u,v=-\frac{N}{2}}^{\frac{N}{2}}\left[e^{\frac{2\pi i}{N}Wv} + e^{-\frac{2\pi i}{N}Wv}\right]g(u,v,E)e^{\frac{2\pi i}{N}(xu+yv)} - \sum_{u,v=-\frac{N}{2}}^{\frac{N}{2}}4g(u,v,E)e^{\frac{2\pi i}{N}(xu+yv)}\right] \quad \textbf{(S17)}$$

$$\nabla_T^2 G(x,y,E) = \frac{1}{N^2}\sum_{u,v=-\frac{N}{2}}^{\frac{N}{2}}\frac{2}{W^2}\left[\cos\left(\frac{2\pi Wu}{N}\right) + \cos\left(\frac{2\pi Wv}{N}\right) - 2\right]g(u,v,E)e^{\frac{2\pi i}{N}(xu+yv)} \quad \textbf{(S18)}$$

With equations S9, S10 and S18, equation S8 is expressed as

$$\frac{1}{N^2}\sum_{u,v=-\frac{N}{2}}^{\frac{N}{2}} f(u,v,E)e^{\frac{2\pi i}{N}(xu+yv)} = \frac{1}{N^2}\sum_{u,v=-\frac{N}{2}}^{\frac{N}{2}}\left[1 - \frac{z_1\Delta\delta(E)}{W^2k(E)\Delta\beta(E)}\left[\cos\left(\frac{2\pi Wu}{N}\right) + \cos\left(\frac{2\pi Wv}{N}\right) - 2\right]\right]g(u,v,E)e^{\frac{2\pi i}{N}(xu+yv)}$$

$$f(u,v,E) = \left[1 - \frac{z_1\Delta\delta(E)}{W^2k(E)\Delta\beta(E)}\left[\cos\left(\frac{2\pi Wu}{N}\right) + \cos\left(\frac{2\pi Wv}{N}\right) - 2\right]\right]g(u,v,E) \quad \textbf{(S19)}$$

$$g(u,v,E) = \frac{f(u,v,E)}{1 - \frac{z_1\Delta\delta(E)}{W^2k(E)\Delta\beta(E)}\left[\cos\left(\frac{2\pi Wu}{N}\right) + \cos\left(\frac{2\pi Wv}{N}\right) - 2\right]} \quad \textbf{(S20)}$$

allowing to estimate $a_2\left(\frac{x}{M},\frac{y}{M}\right)$ from $g(u,v,E)$ in equation S10 as

$$e^{-2k(E)\Delta\beta(E)a_2\left(\frac{x}{M},\frac{y}{M}\right)} = \frac{1}{N^2}\sum_{u,v=-\frac{N}{2}}^{\frac{N}{2}}\left[\frac{f(u,v,E)}{1 - \frac{z_1\Delta\delta(E)}{W^2k(E)\Delta\beta(E)}\left[\cos\left(\frac{2\pi Wu}{N}\right) + \cos\left(\frac{2\pi Wv}{N}\right) - 2\right]}\right]e^{\frac{2\pi i}{N}(xu+yv)}$$

$$a_2\left(\frac{x}{M},\frac{y}{M}\right) = -\frac{1}{2k(E)\Delta\beta(E)}\ln\left[\frac{1}{N^2}\sum_{u,v=-\frac{N}{2}}^{\frac{N}{2}}\left[\frac{f(u,v,E)}{1 - \frac{z_1\Delta\delta(E)}{W^2k(E)\Delta\beta(E)}\left[\cos\left(\frac{2\pi Wu}{N}\right) + \cos\left(\frac{2\pi Wv}{N}\right) - 2\right]}\right]e^{\frac{2\pi i}{N}(xu+yv)}\right] \quad \textbf{(S21)}$$

Verification

Monochromatic images were acquired for a PMMA tube (diameters of 1.94, 2.93 and 3.85 mm) with an inner tube (diameters of 0.92, 1.85 and 2.82 mm), made of Blood, Air and P. Iodine. The corresponding imaging energies were 12 keV and 18 keV, a sample-detector of 0.6 m (z_1), and an X-ray source-sample distance of 1.2. The objective is to retrieve the projected thickness of Blood, Air and P. Iodine ($\Delta\delta(E) = \delta_{Materials}(E) - \delta_{PMMA}(E)$ and $\Delta\beta(E) = \beta_{Material}(E) - \beta_{PMMA}(E)$) using equation S21. The pixel size was $W = 55\ \mu$m.

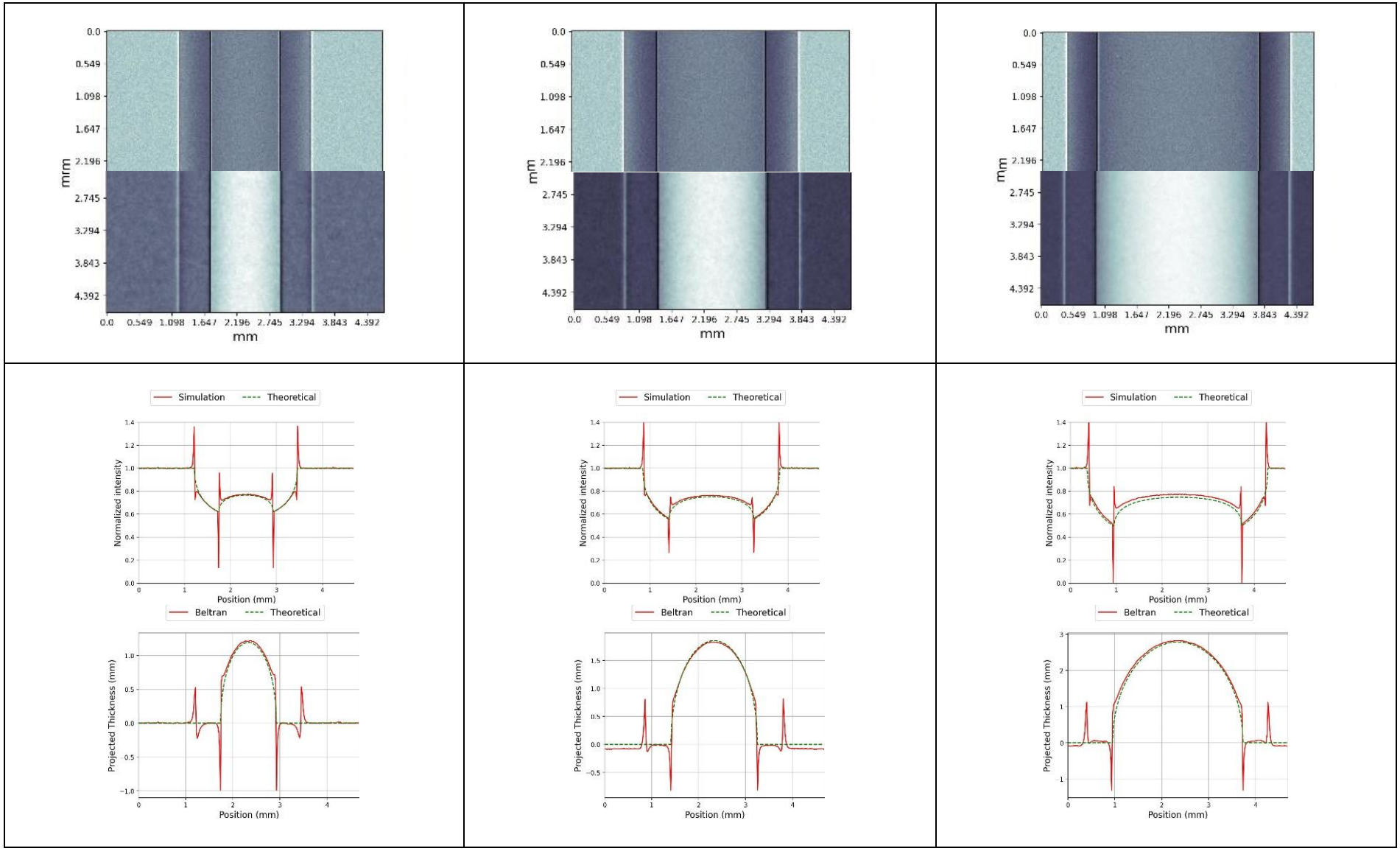

Figure S1. Images acquired at 12 keV using Inline XPCI with the lumen filled with air, along with the projected lumen thickness retrieved using Equation S21.

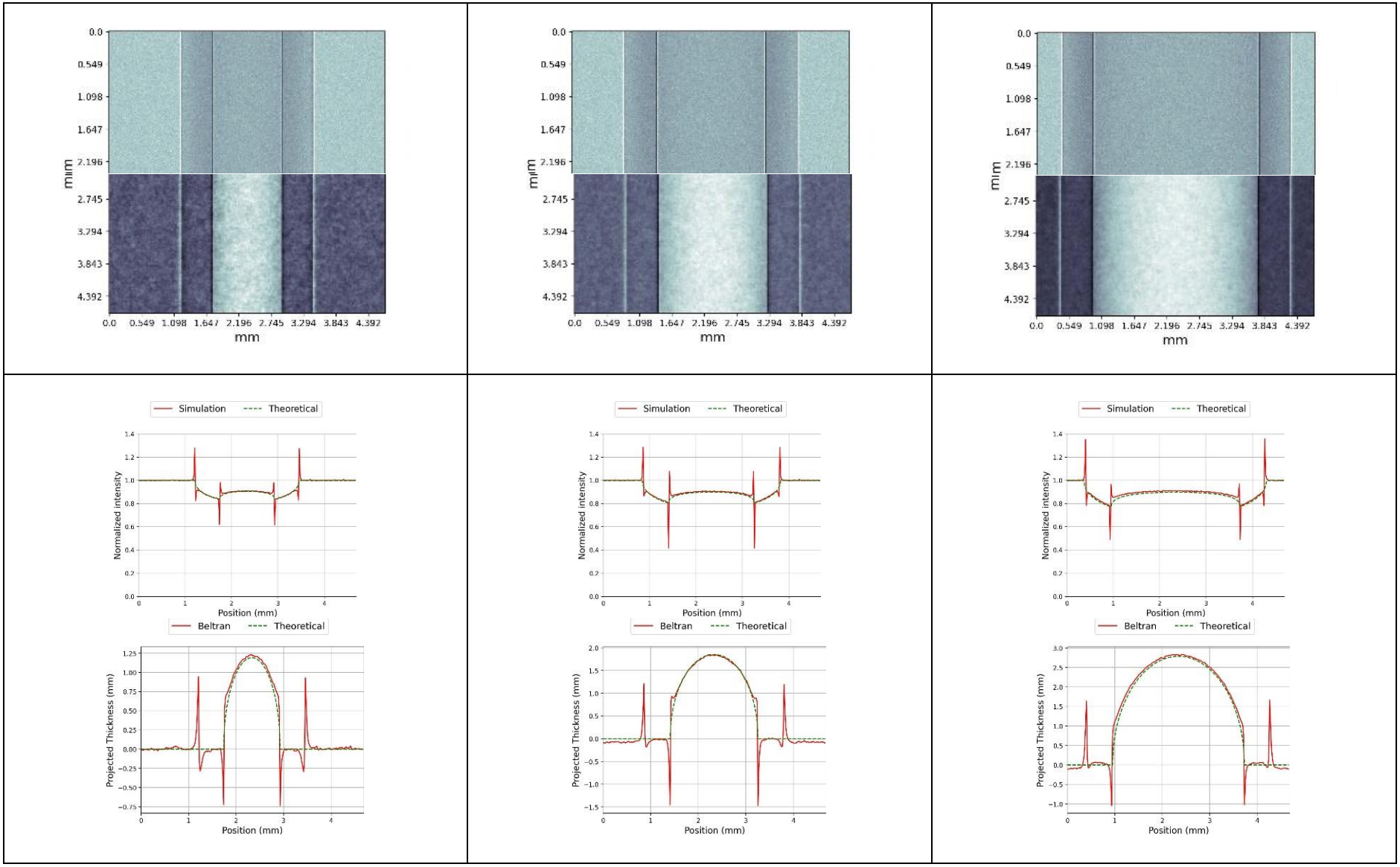

Figure S2. Images acquired at 18 keV using Inline XPCI with the lumen filled with air, along with the projected lumen thickness retrieved using Equation S21.

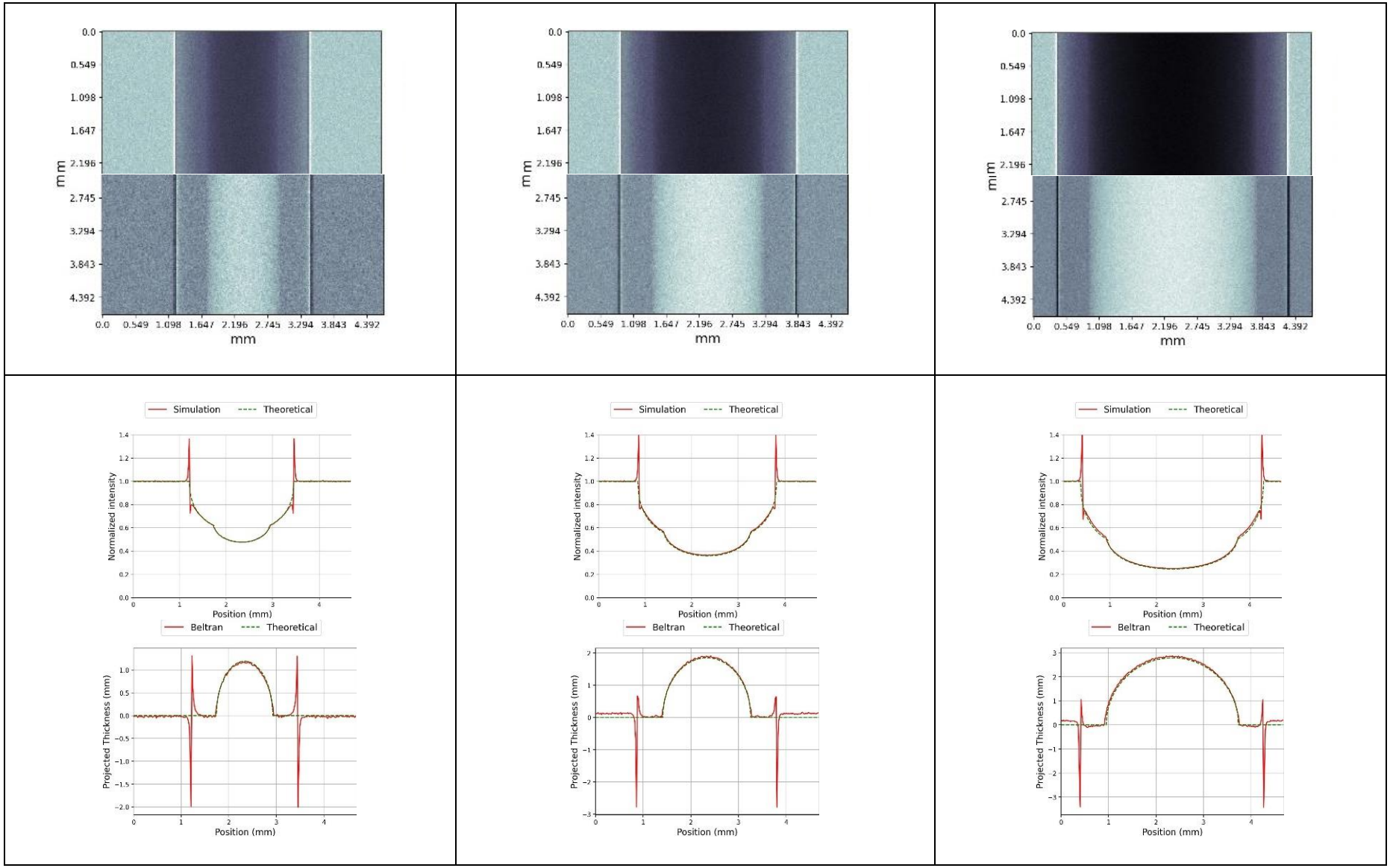

Figure S3. Images acquired at 12 keV using Inline XPCI with the lumen filled with blood, along with the projected lumen thickness retrieved using Equation S21.

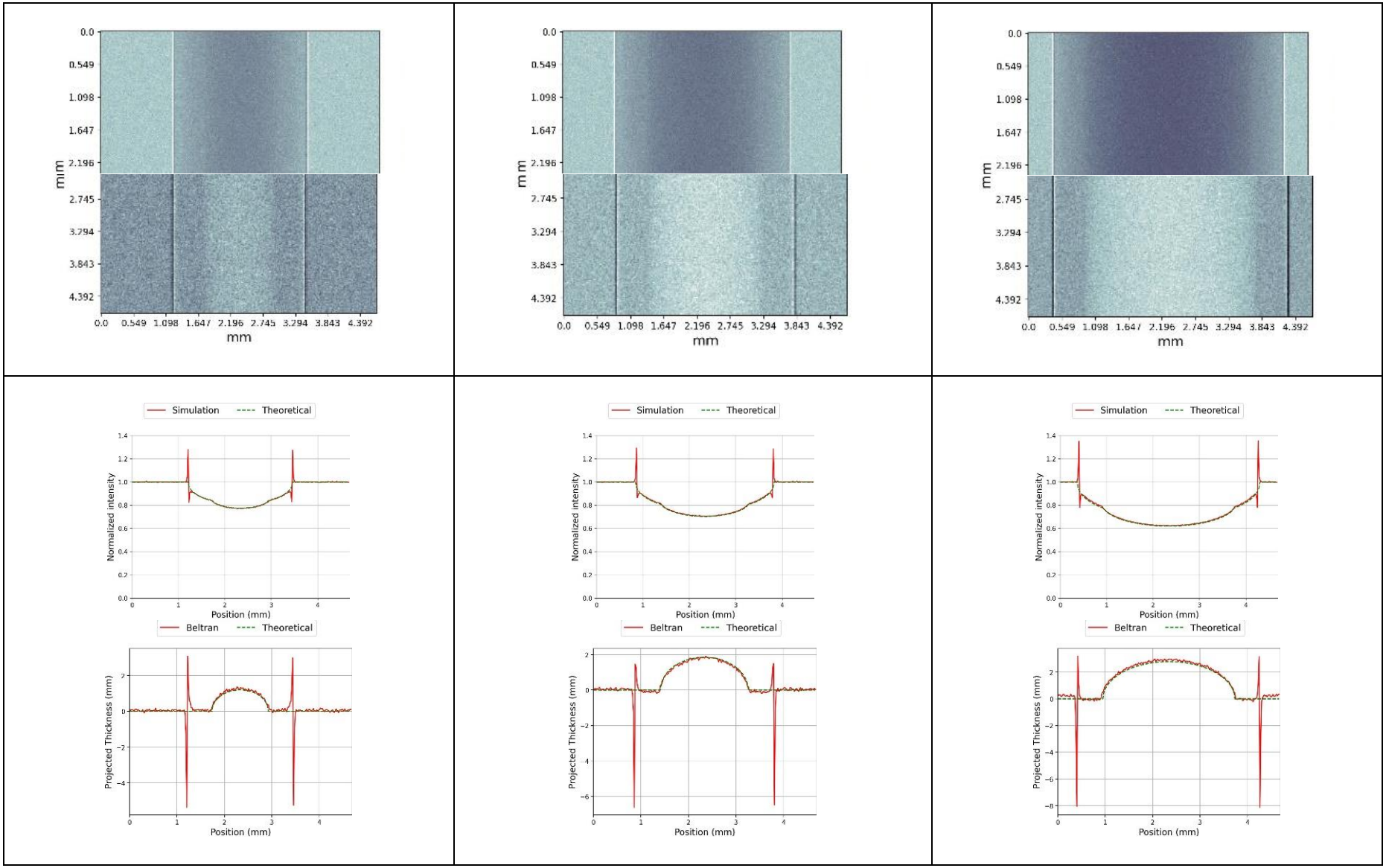

Figure S4. Images acquired at 18 keV using Inline XPCI with the lumen filled with blood, along with the projected lumen thickness retrieved using Equation S21.

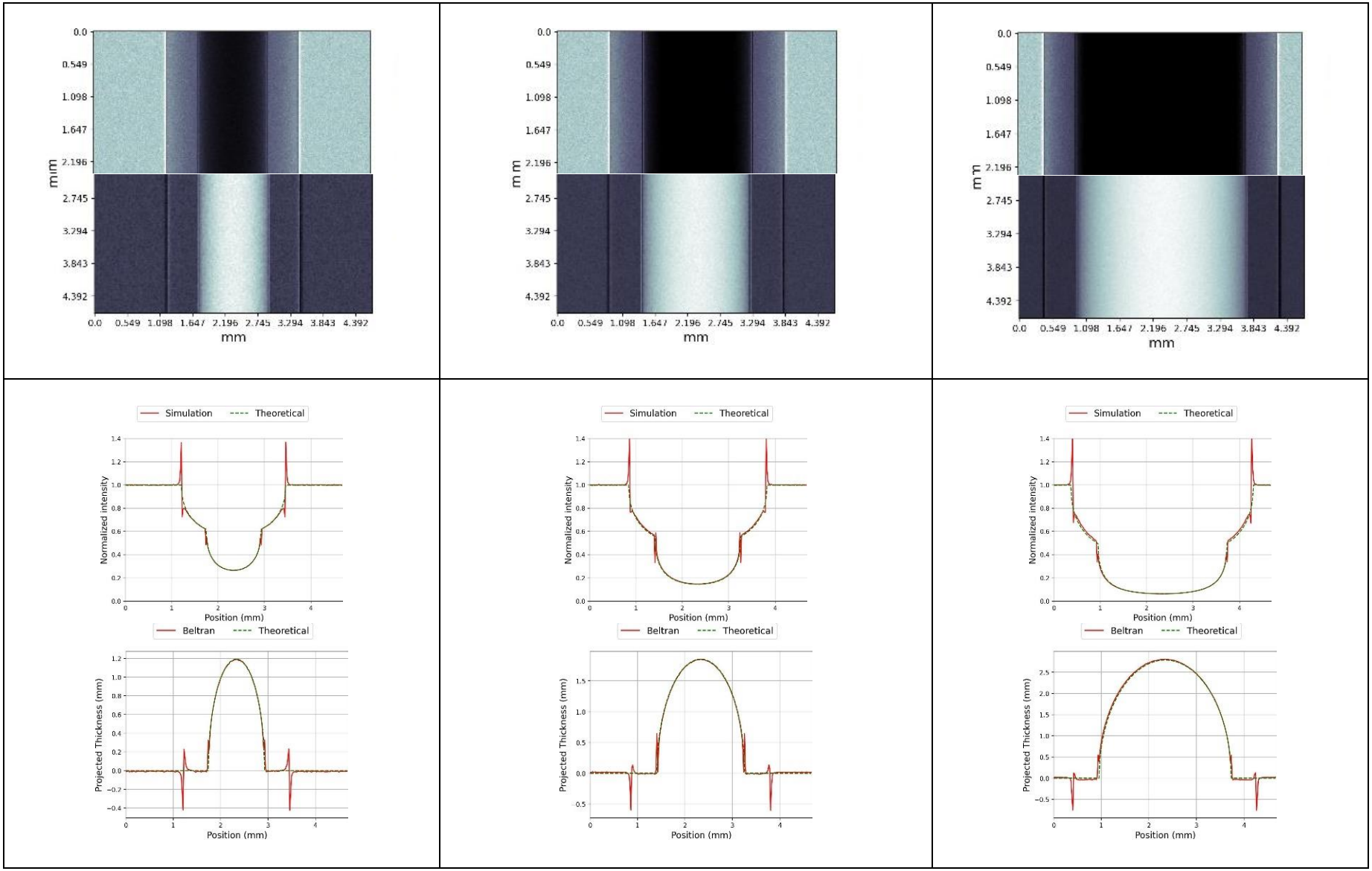

Figure S5. Images acquired at 12 keV using Inline XPCI with the lumen filled with P.Iodine, along with the projected lumen thickness retrieved using Equation S21.

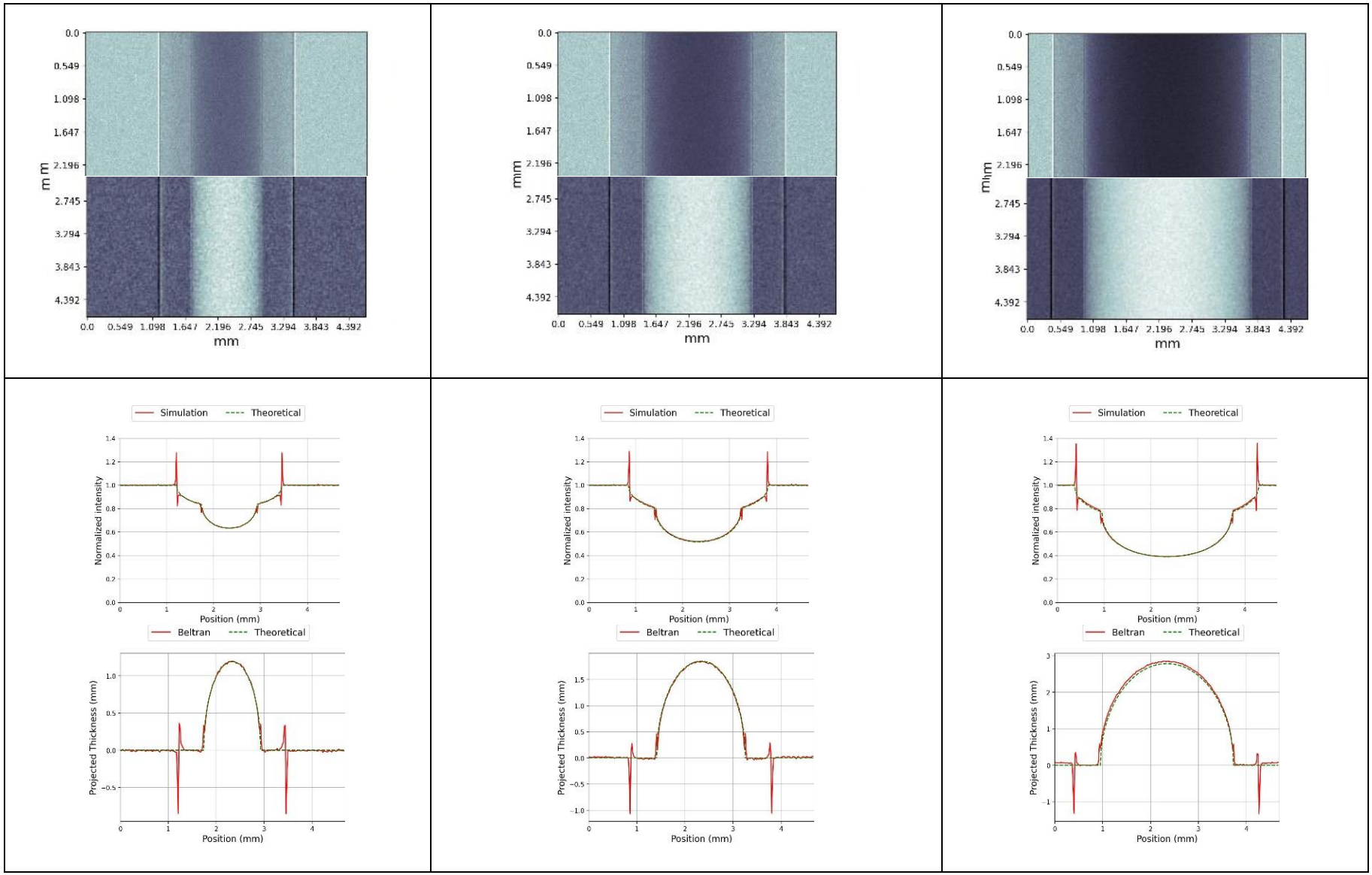

Figure S6. Images acquired at 18 keV using Inline XPCI with the lumen filled with P.Iodine, along with the projected lumen thickness retrieved using Equation S21.

2. Results-First sample

a. Air (Experimental-Simulation)

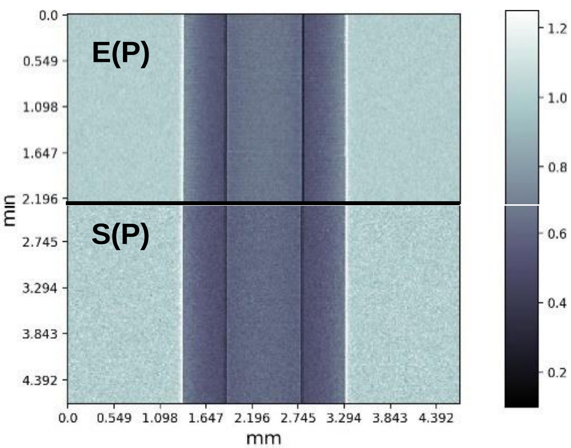

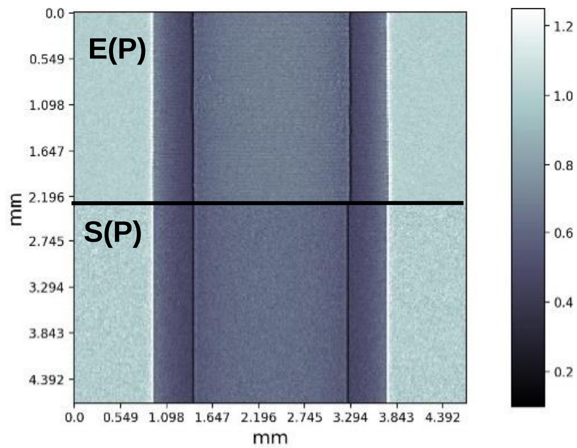

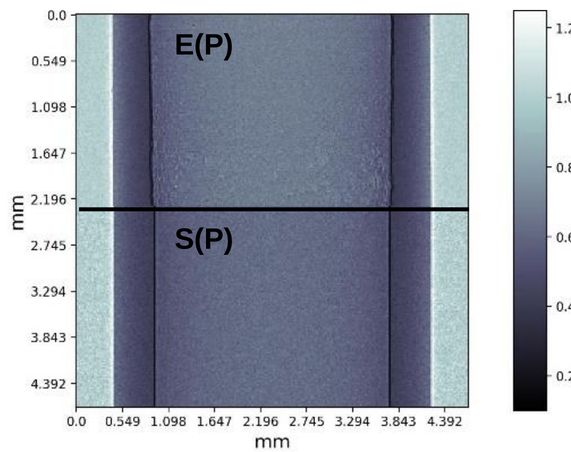

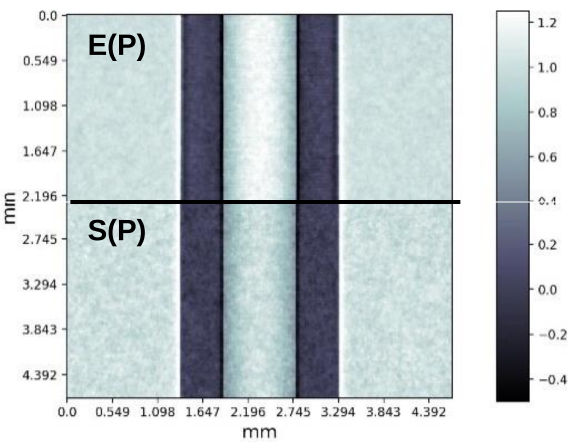

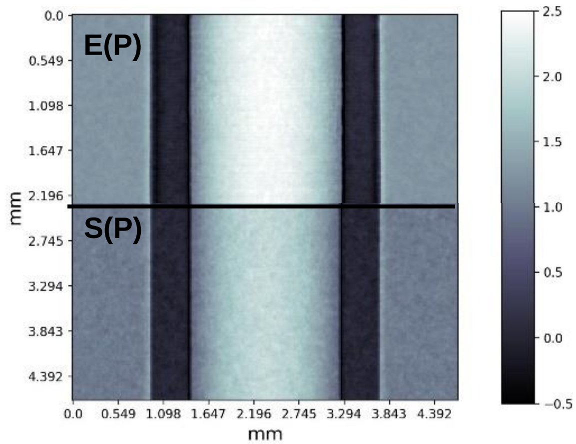

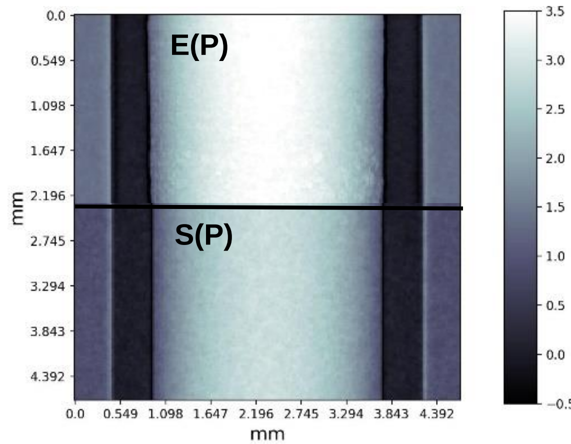

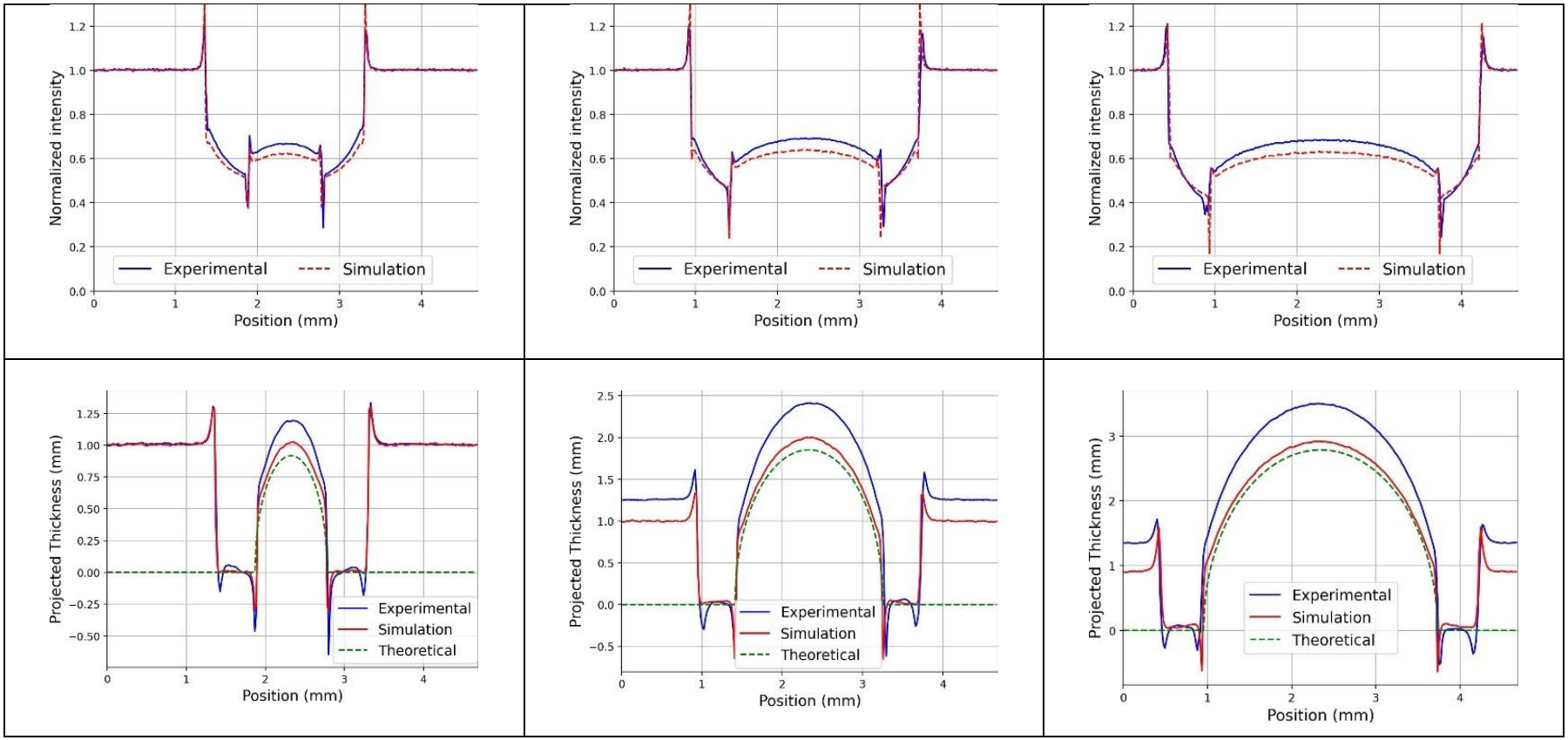

Figure S7. Experimental-E(P) (Simulation-S(P)) CI (first row) and lumen projected thickness (second row) for internal diameter PMMA tubes filled with air. Comparison of CI (third row) and lumen projected thickness (fourth row) profiles of simulation and experimental results for all internal diameter PMMA tubes. The green dashed profiles represent the expected lumen profile.

b. Blood (Experimental-Simulation)

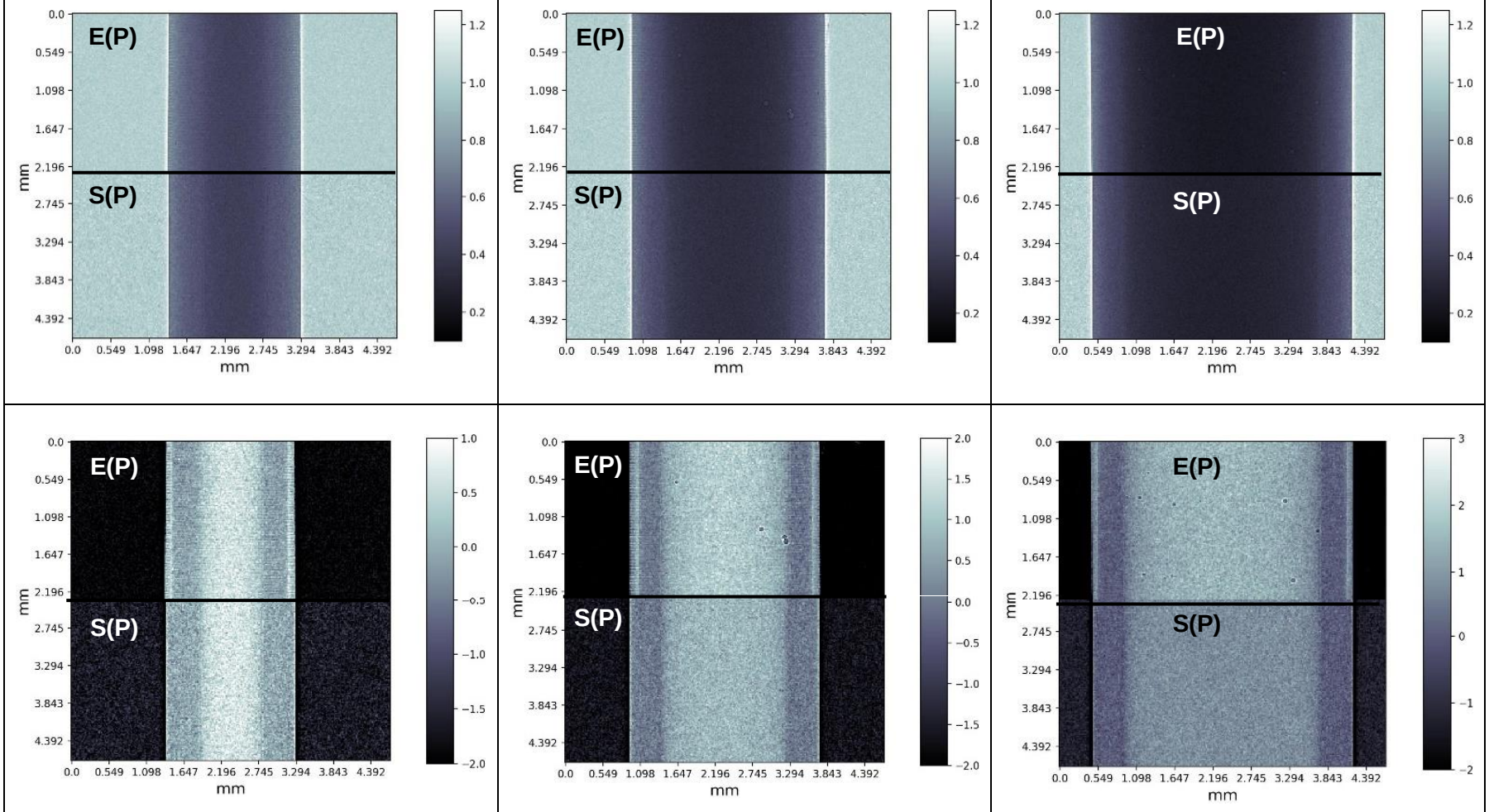

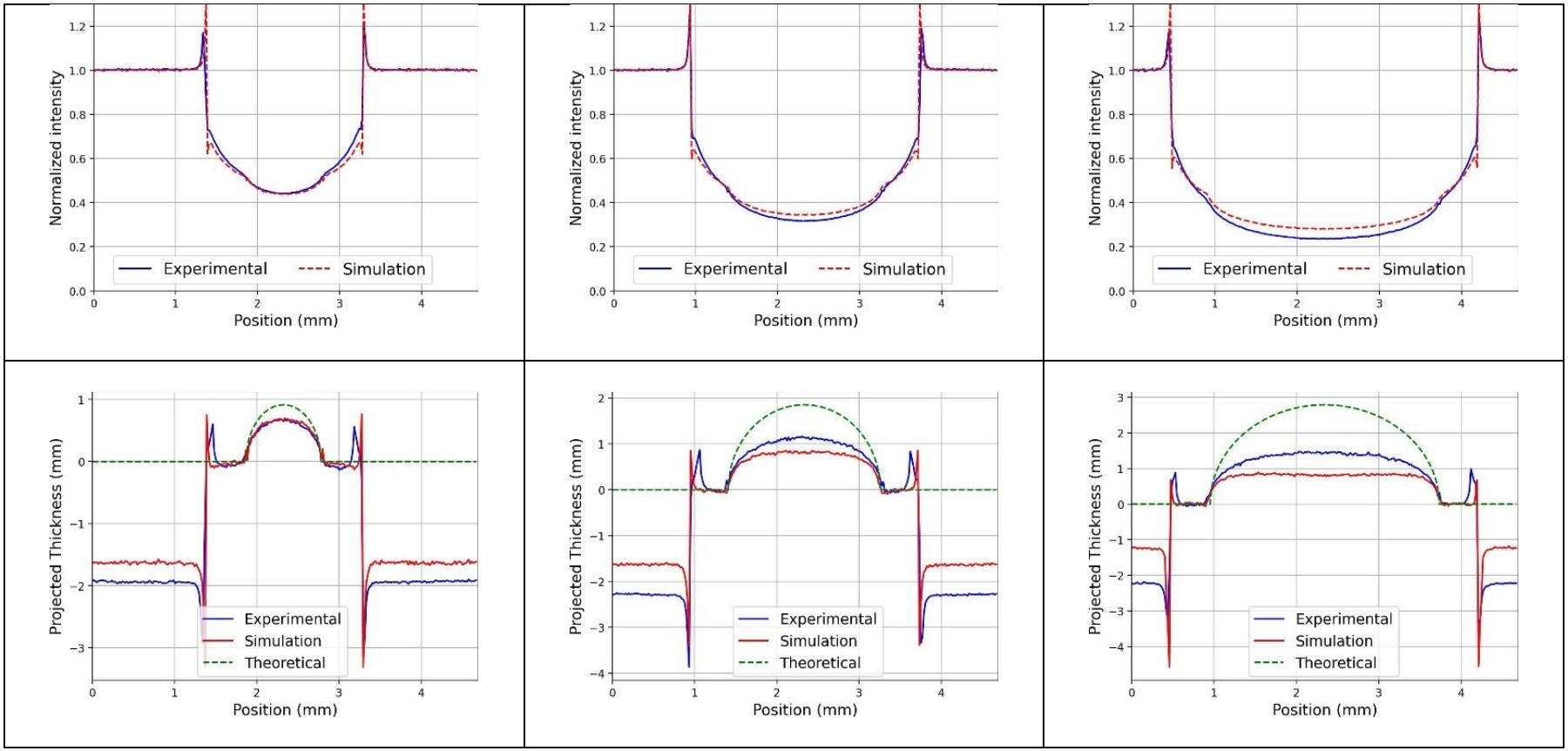

Figure S8. Experimental-E(P) (Simulation-S(P)) CI (first row) and lumen projected thickness (second row) for internal diameter PMMA tubes filled with blood. Comparison of CI (third row) and lumen projected thickness (fourth row) profiles of simulation and experimental results for all internal diameter PMMA tubes. The green dashed profiles represent the expected lumen profile.

c. P. Iodine (Experimental-Simulation)

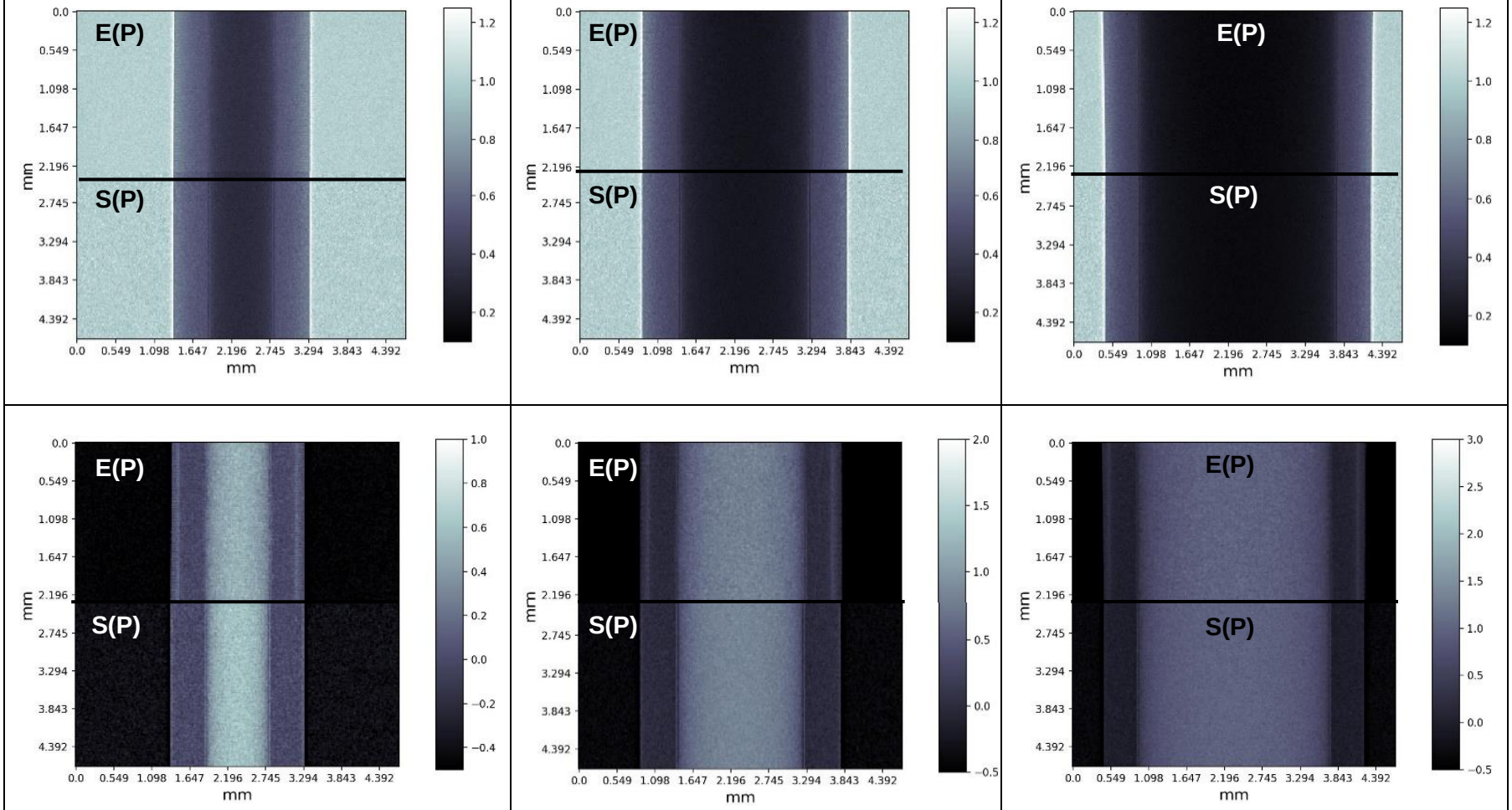

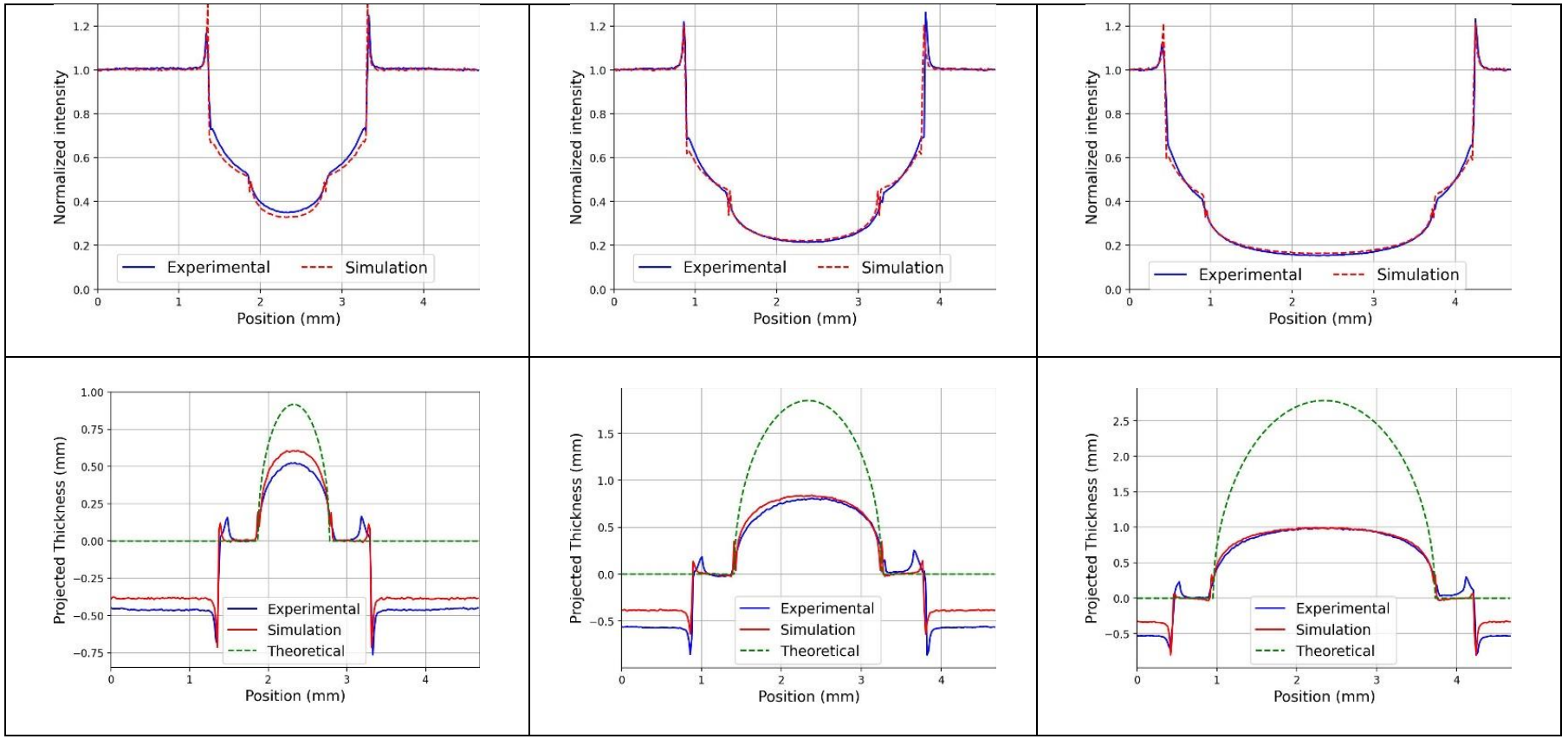

Figure S9. Experimental-E(P) (Simulation-S(P)) CI (first row) and lumen projected thickness (second row) for internal diameter PMMA tubes filled with P. iodine. Comparison of CI (third row) and lumen projected thickness (fourth row) profiles of simulation and experimental results for all internal diameter PMMA tubes. The green dashed profiles represent the expected lumen profile.

d. Air (Simulation)

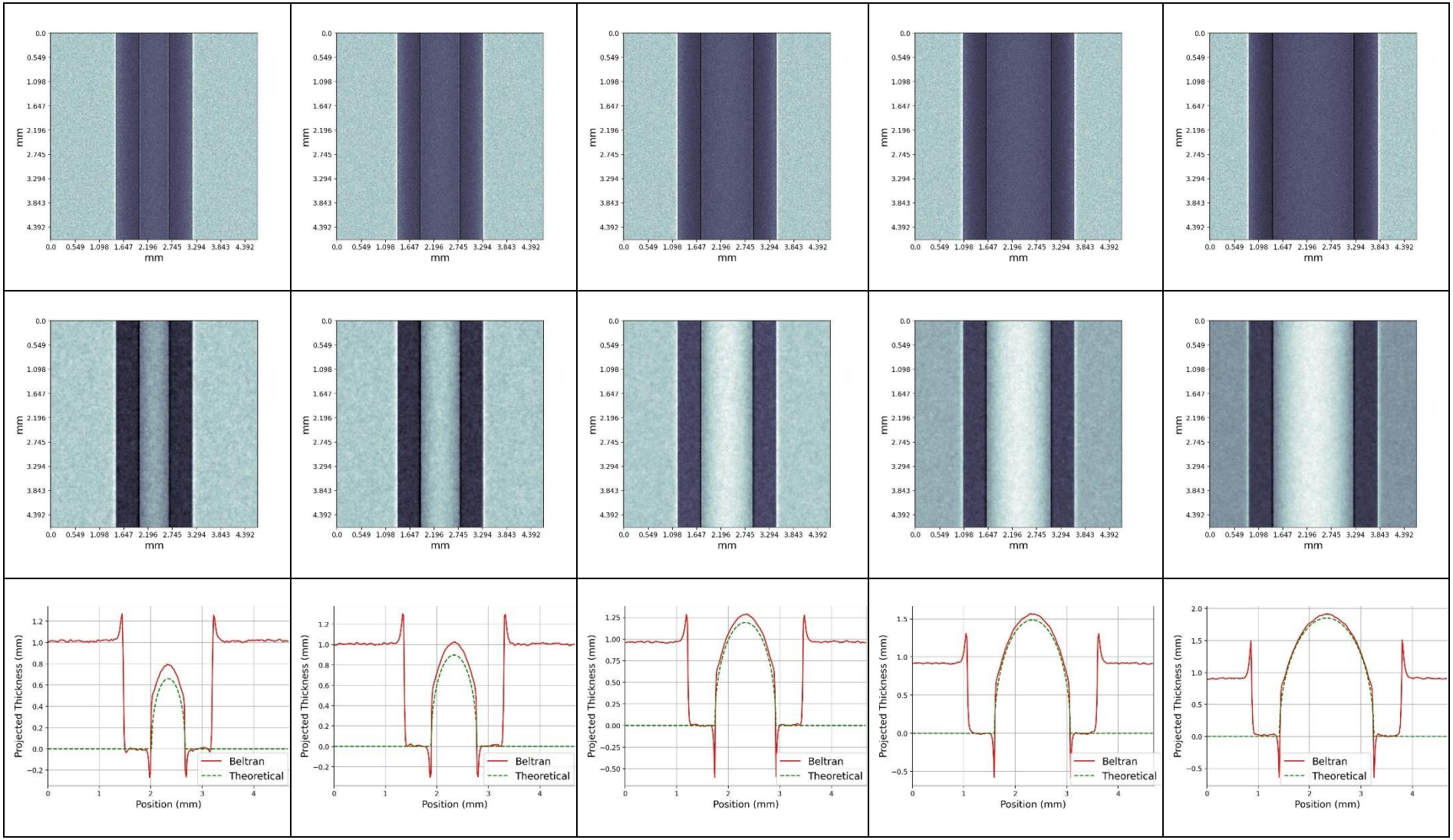

Figure S10. Simulation-S(P) CI (first row) and lumen projected thickness (second row) for internal diameter PMMA tubes filled with air. Lumen projected thickness (third row) profiles of simulation results for all internal diameter PMMA tubes. The green dashed profiles represent the expected lumen profile.

e. Blood (Simulation)

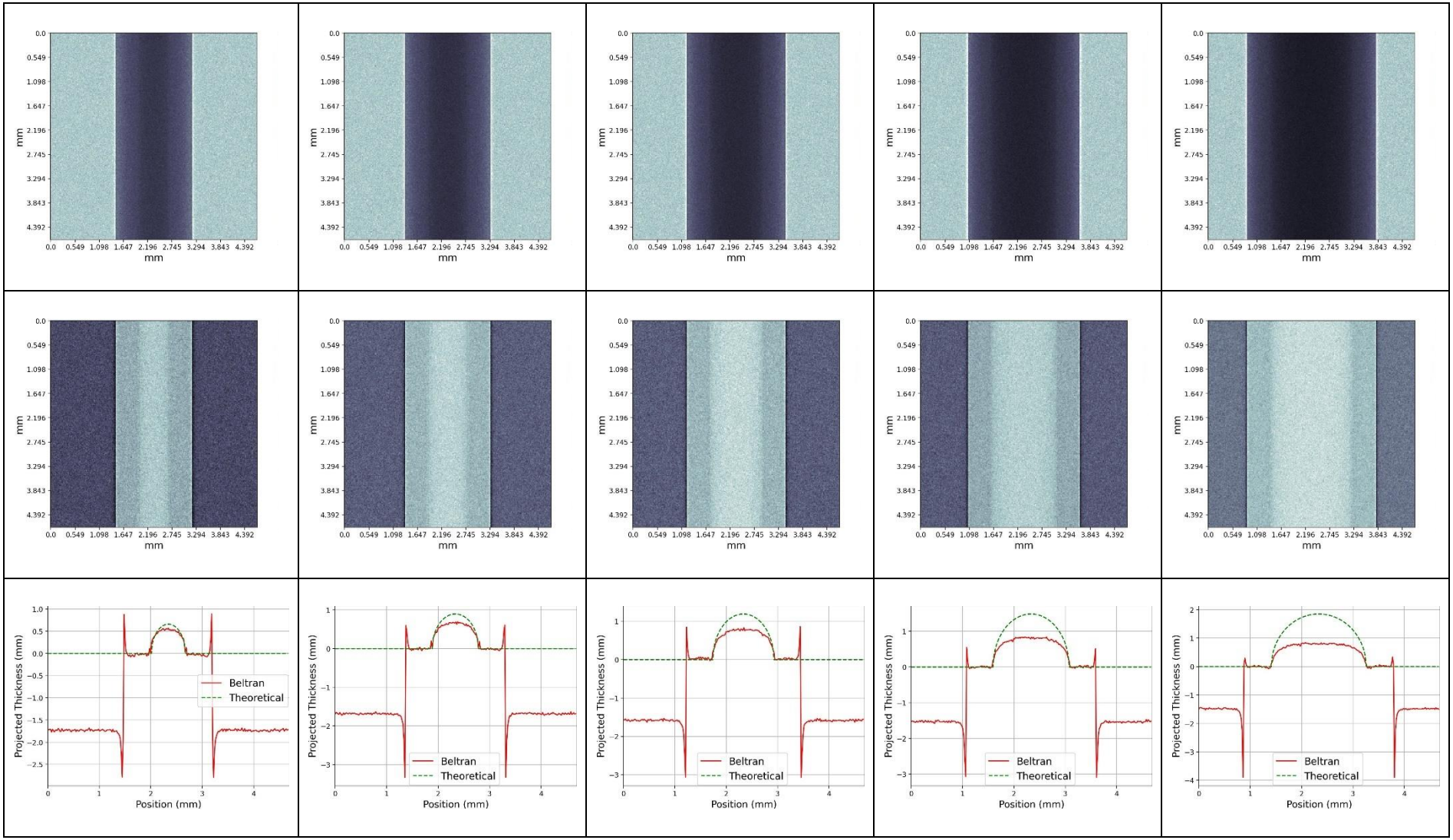

Figure S11. Simulation CI (first row) and lumen projected thickness (second row) for internal diameter PMMA tubes filled with blood. Lumen projected thickness (third row) profiles of simulation results for all internal diameter PMMA tubes. The green dashed profiles represent the expected lumen profile.

f. P. Iodine (Simulation)

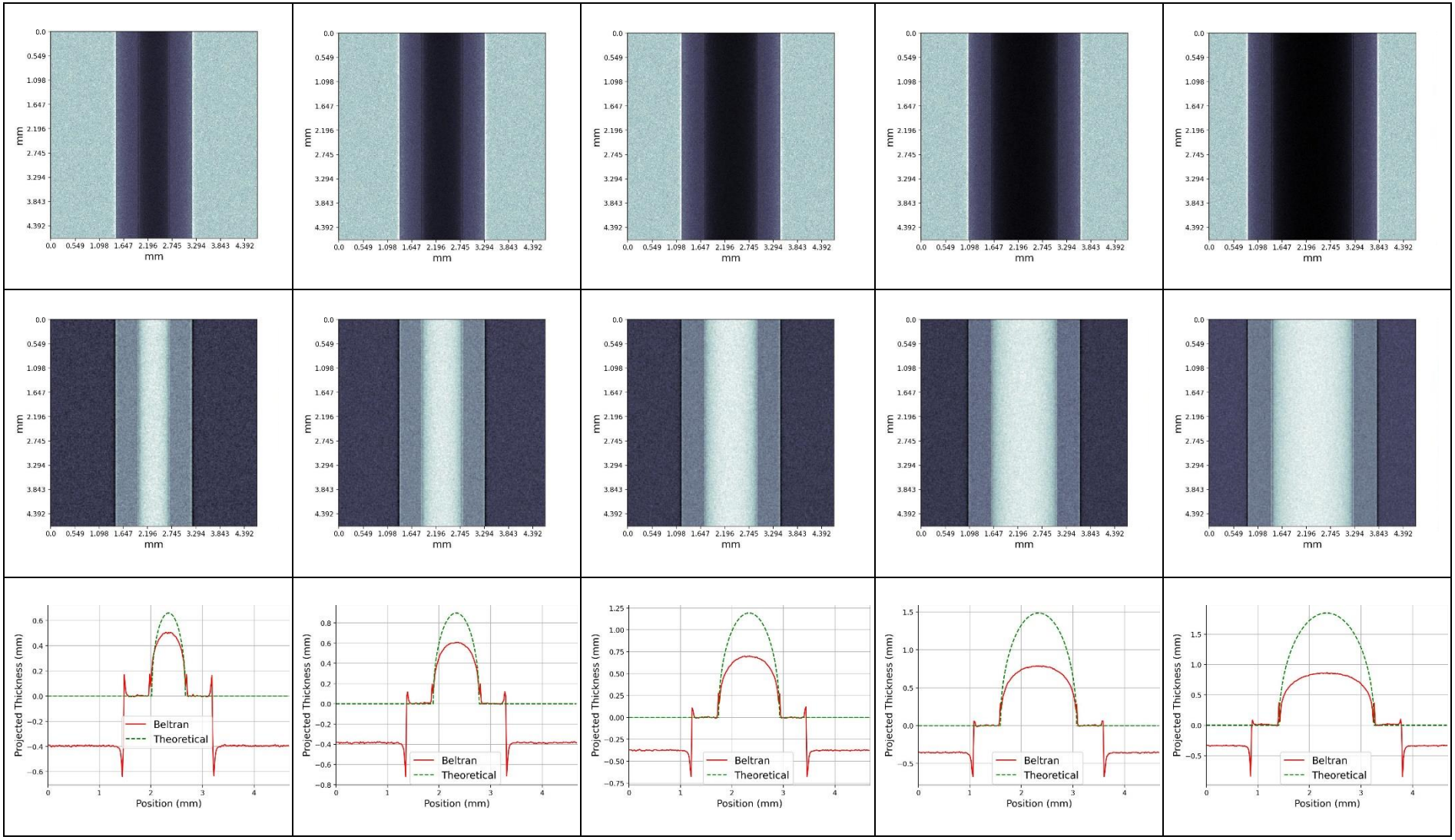

Figure S12. Simulation CI (first row) and lumen projected thickness (second row) for internal diameter PMMA tubes filled with P.Iodine. Lumen projected thickness (third row) profiles of simulation results for all internal diameter PMMA tubes. The green dashed profiles represent the expected lumen profile.

3. Choice of the Tikhonov regularization parameter

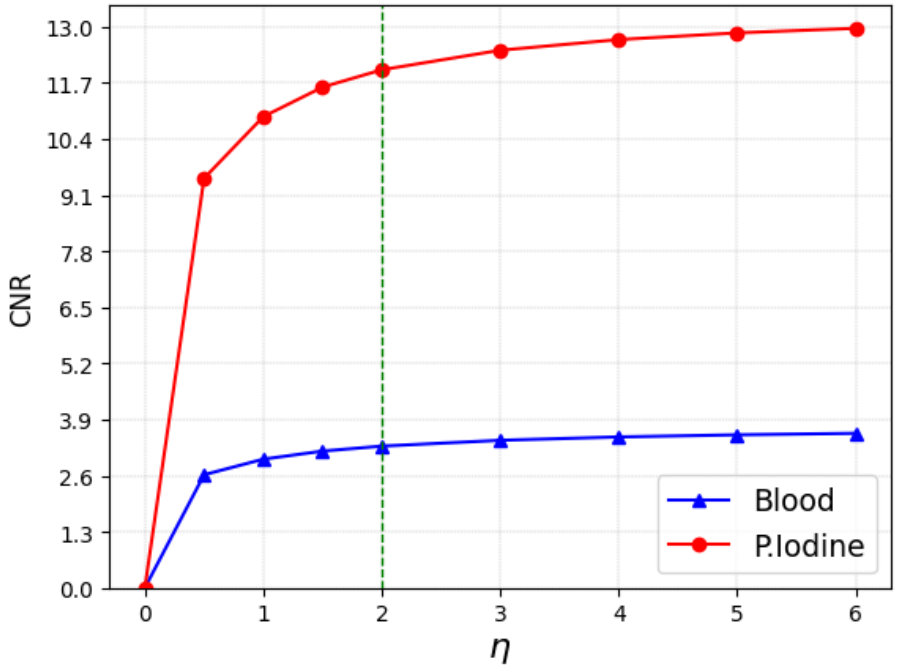

Figure S13. CNR values of the lumen's projected thickness maps obtained using different regularization parameters. The measurements correspond to tubes with an external diameter of 1.94 mm filled with blood and P. iodine.

4. Recovering projected thickness maps at energies other than the average energy

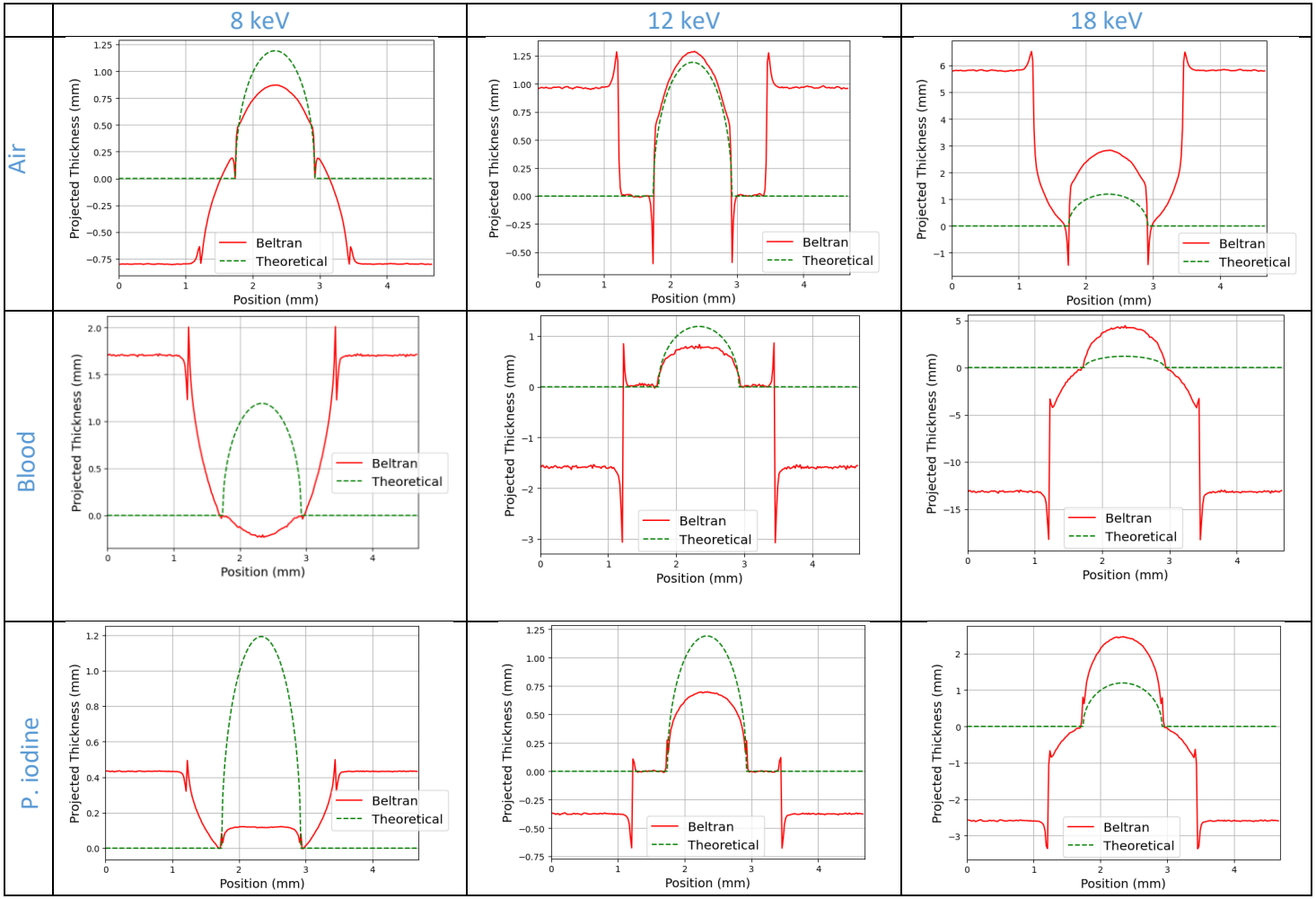

Figure S14. Projected thickness profiles for Air, Blood and P. Iodine recovered at energies of 8 keV, 12 keV and 18 keV.

For $E \neq 12$ keV, the projected thickness in the tube wall region is not constant and appears irregular for all materials. Furthermore, for $E < 12$ keV, negative thickness values are observed in the lumen region for blood, and the estimated thicknesses are significantly underestimated. For $E > 12$ keV, the estimated thicknesses are overestimated.